Supporting Information

Rational Design of Mixed-Valence Cobalt-Based Nanowires via Simultaneous Vanadium and Iron Modulations for Enhanced Alkaline Electrochemical Water Splitting

Weijiang Gan,[a,†] Selvam Mathi,[b,†] Jingting Li,[b] Adewale K. Ipadeola,[c] Jianqiu Deng,[d] Aboubakr M. Abdullah,[c] M.-Sadeeq Balogun,*[,a,b,d] Zhongmin Wang*[,a,d]

[a]State Key Laboratory of Non-Food Biomass and Enzyme Technology, Guangxi Academy of Sciences, Nanning, Guangxi 530007, China.

[b]College of Materials Science and Engineering, Hunan Joint International Laboratory of Advanced Materials and Technology for Clean Energy, Hunan University, Changsha, 410082, People's Republic of China.

[c]Center for Advanced Materials, Qatar University, Doha 2713, Qatar.

[d]Guilin University of Electronic Technology Guilin 541004, P. R. China

[1]These authors contributed equally

E-mail: zmwang@mail.gxas.cn; balogun@hnu.edu.cn

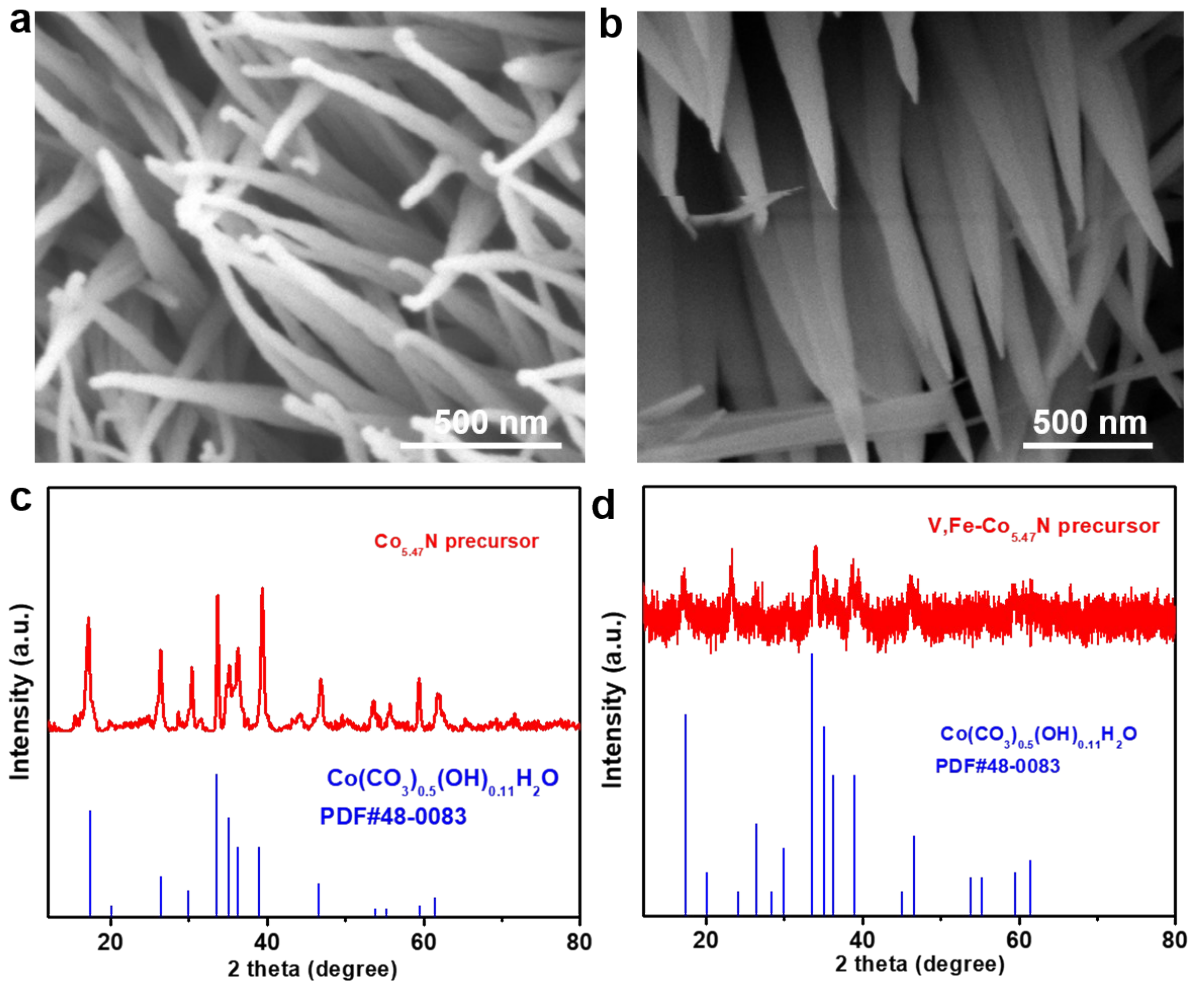

Figure S1. SEM images of (a) V, Fe-$Co_{5.47}N$ and (b) $Co_{5.47}N$ precursors. XRD spectra of (c) $Co_{5.47}N$ and (d) V, Fe-$Co_{5.47}N$ precursors.

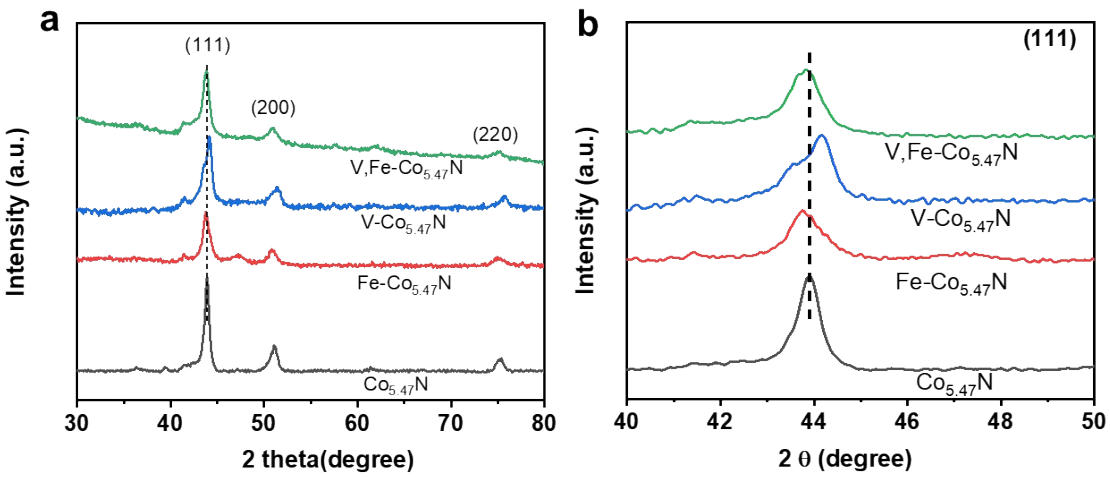

Figure S2. The XRD patterns of $Co_{5.47}N$, V-$Co_{5.47}N$, Fe-$Co_{5.47}N$ and V,Fe-$Co_{5.47}N$ catalysts.

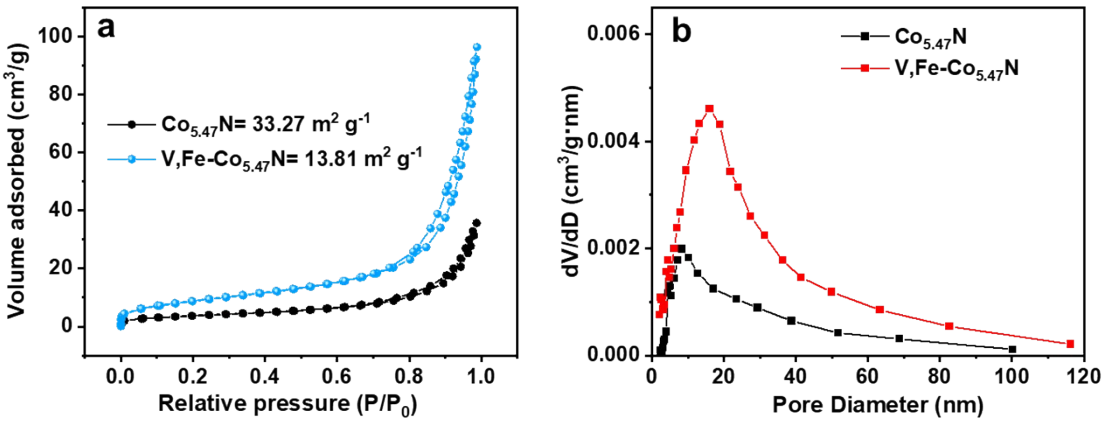

Figure S3. N_2 adsorption-desorption isotherm curves of $Co_{5.47}N$ and V, Fe-$Co_{5.47}N$.

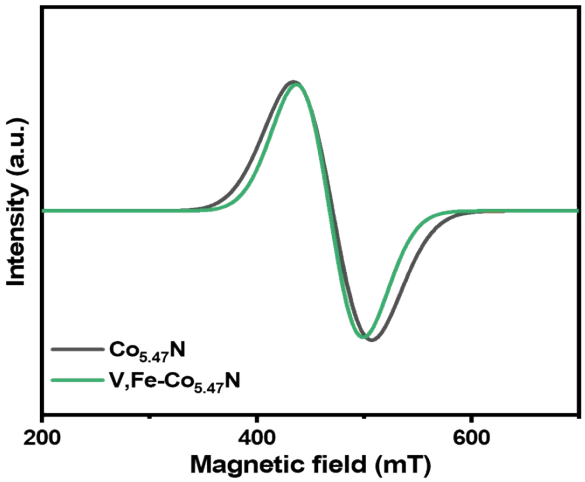

Figure S4. The EPR spectroscopy of $Co_{5.47}N$, V-$Co_{5.47}N$, Fe-$Co_{5.47}N$, and V,Fe-$Co_{5.47}N$.

The EPR spectra were performed at room temperature using a Bruker Elexsys 500 EPR spectrometer operating at the X-band frequency (≈9.491 GHz) with a field modulation frequency of 100 kHz. The magnetic field was scanned in the range of 500–6500 G and the used microwave power was 0.64 mW. A powder sample of 100 mg was taken in a quartz tube for EPR measurements. EPR spectra were measured to illustrate the presence of vacancies in the synthesized samples.

(a)

Element	Wt%	Atomic %
N	13.89	35.56
Fe	1.48	3.27
Co	83.57	58.08
V	1.06	3. 09
Total:	100.00	100.00

(b)

Element	Wt%	Atomic %
P	4.24	7.71
Fe	2.59	2.61
Co	89.54	85.66
V	3.63	4.02
Total:	100.00	100.00

Figure S5. Element contents for V, Fe-$Co_{5.47}N$ and V, Fe-CoP

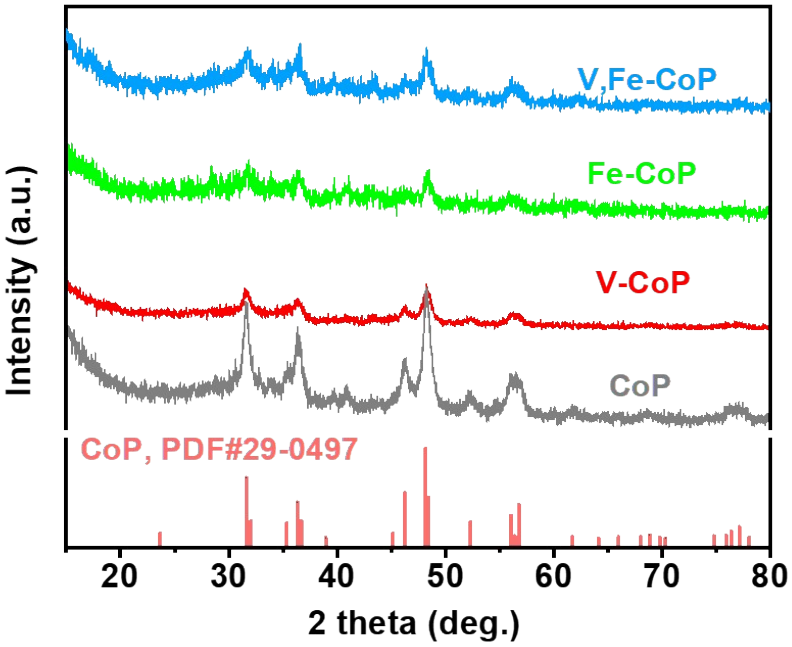

Figure S6. The XRD patterns of $Co_{5.47}N$, V-$Co_{5.47}N$, Fe-$Co_{5.47}N$ and V, Fe-$Co_{5.47}N$ catalysts.

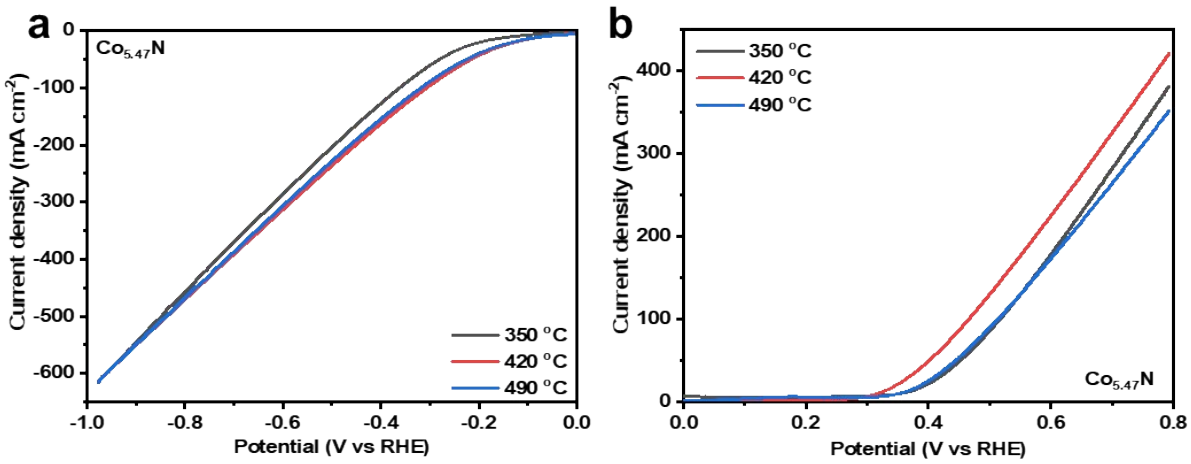

Figure S7. (a) HER and (b) OER LSV curves of $Co_{5.47}N$ at different temperatures.

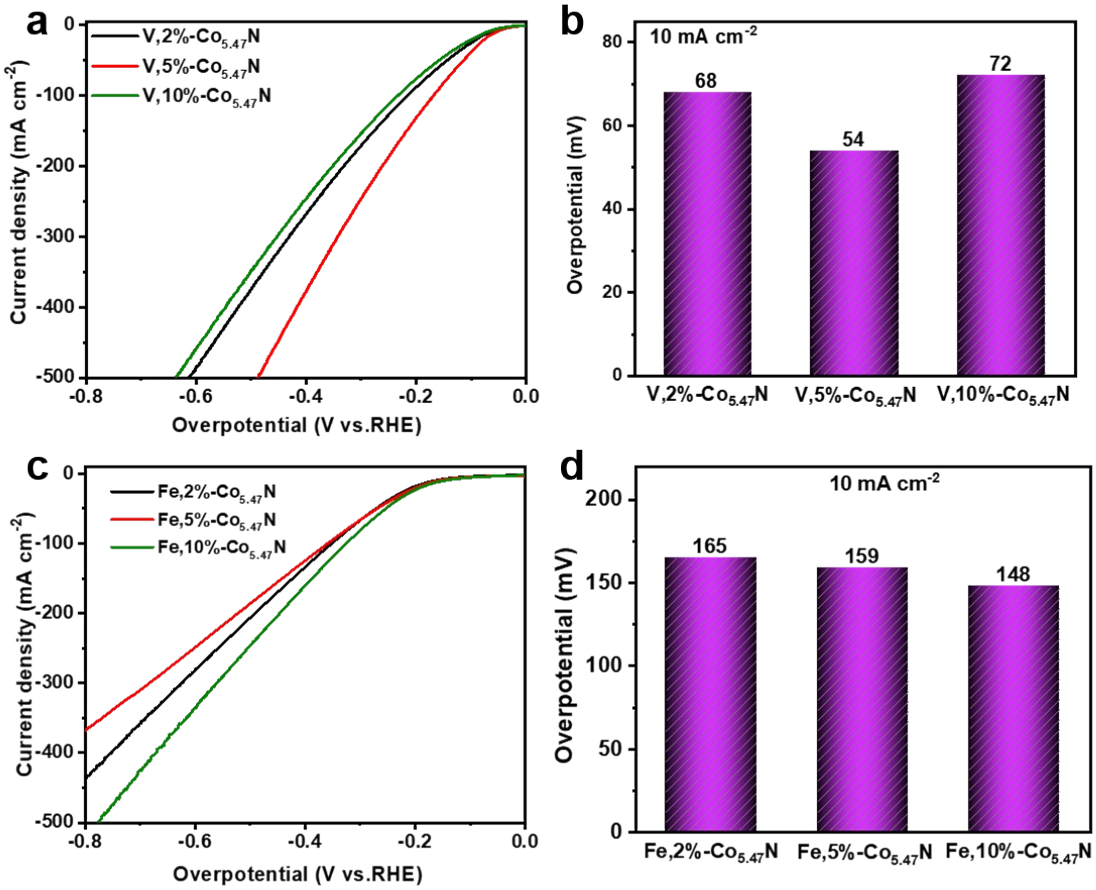

Figure S8. (a) Polarization curves and (b) overpotentials of various V-$Co_{5.47}N$ samples at 10 mA cm^{-2} for HER. (c) Polarization curves and (d) overpotentials of various Fe-$Co_{5.47}N$ samples at 10 mA cm^{-2} for HER.

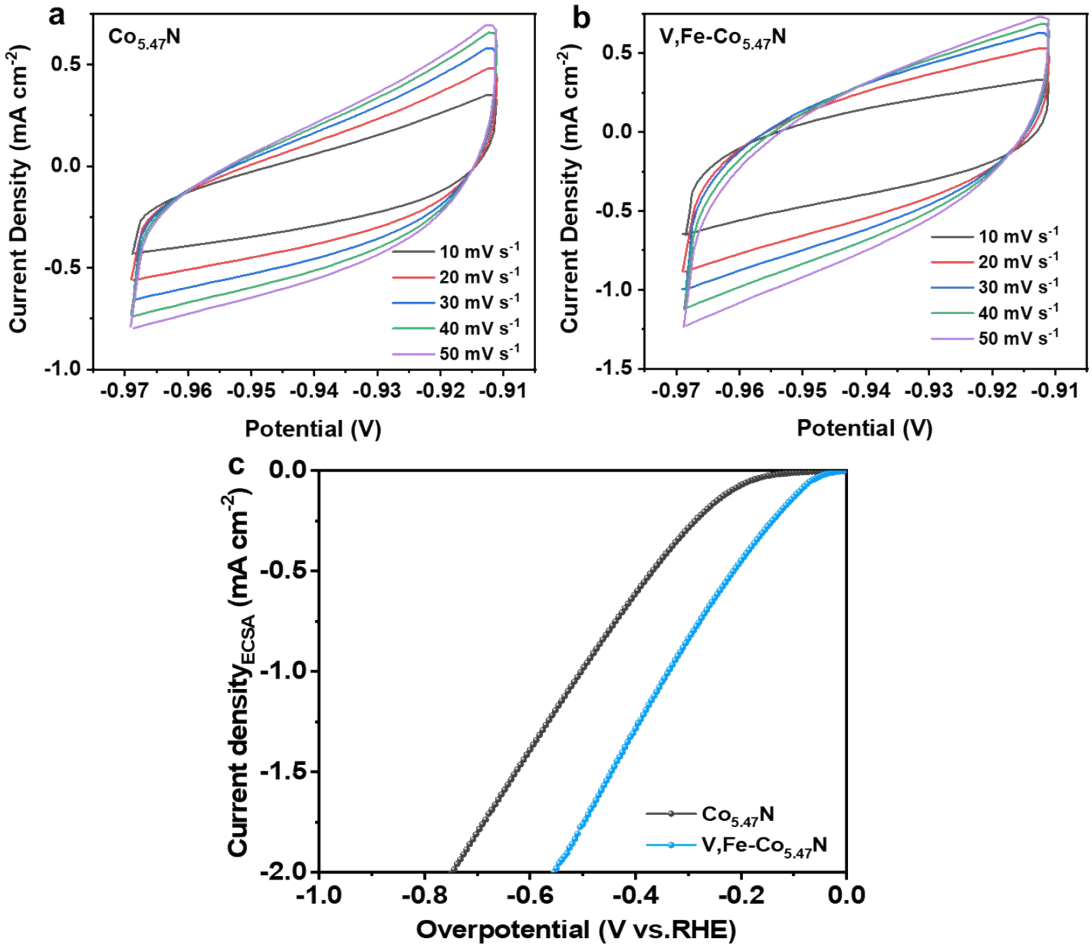

Figure S9. CV curves (a) $Co_{5.47}N$ and (b) V, Fe-$Co_{5.47}N$ in the double layer capacitive region at the scan rates of 10 mV s^{-1} to 50 mV s^{-1} for HER. (c) HER Normalized ECSA.

The electrochemical active surface area (ECSA) of the catalysts was estimated by measuring the electrochemical double-layer capacitance (C_{dl}) using cyclic voltammetry (CV) curves under a potential window of -0.97 ~ -0.91 V vs HER and 0.18 ~ 0.23 V vs OER at scanning rates of 10, 20, 30, 40 and 50 mV s^{-1} in the non-Faradaic potential region. The C_{dl} of various catalysts were equivalent to the linear slope, which was obtained by plotting the $\Delta J/2$ at different potential against the scan rate. $\Delta J/2$ was calculated using the following equation:

$$\Delta j/2 = (j_{anodic} - j_{cathodic})/2 \quad (3)$$

Then, ECSA was calculated as follows:

$$ECSA = C_{dl}/C_s \quad (4)$$

Here, C_s=40 μF/cm^2, according to that the specific capacitance for a flat surface was generally found to be in the range of 20-60 μF cm^{-2}.

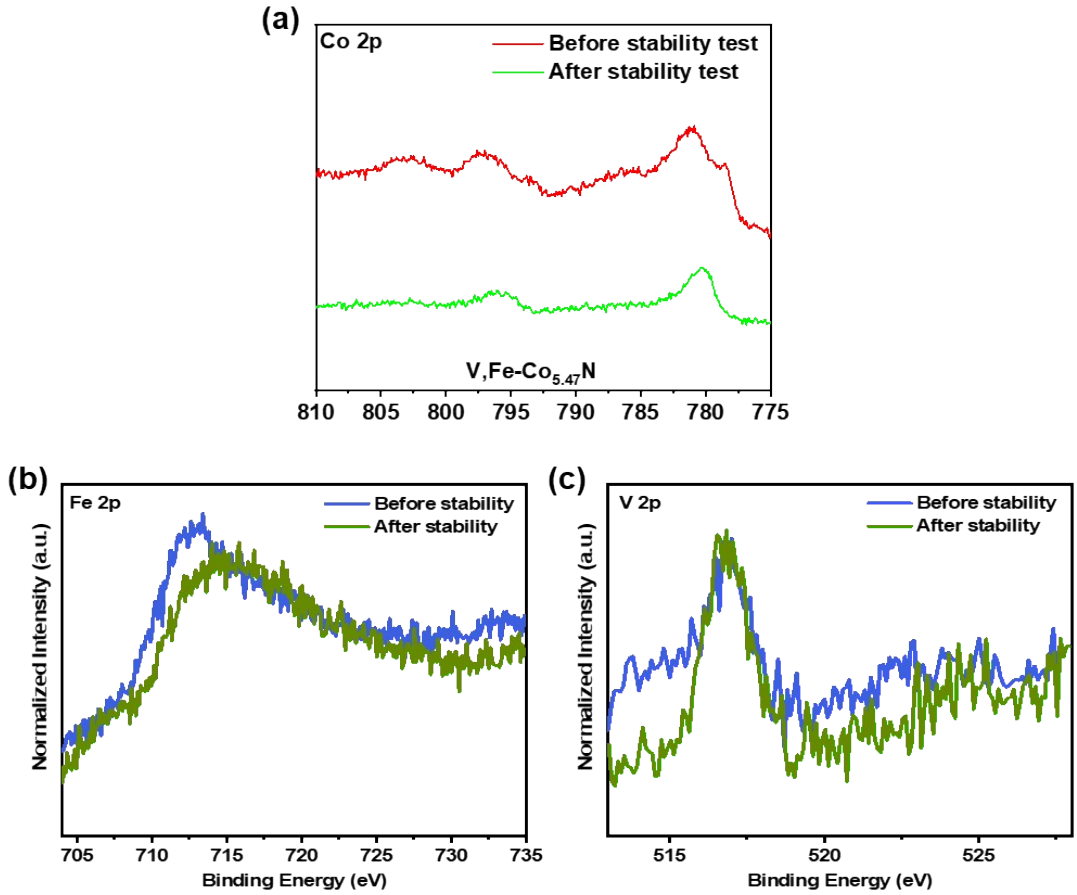

Figure S10. (a) Co 2p, (b) Fe 2p, and (c) V 2p XPS spectra of V, Fe-$Co_{5.47}N$ before and after the stability test.

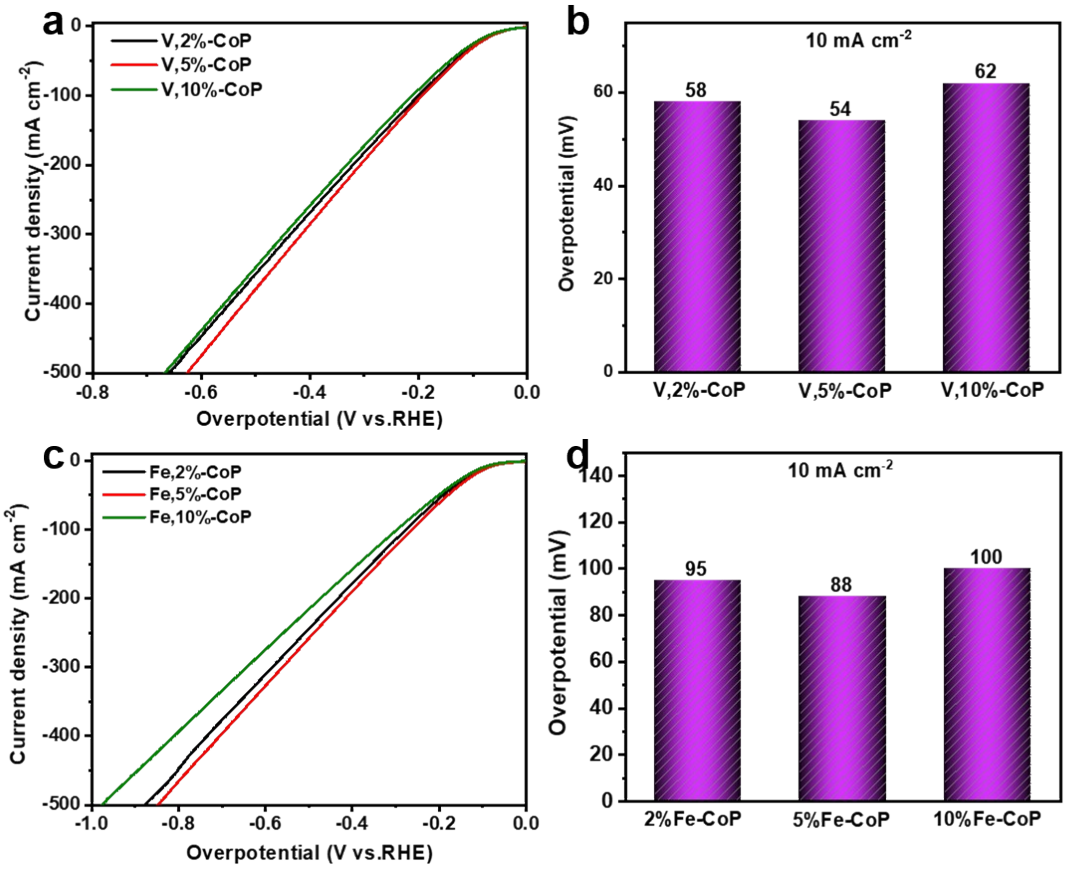

Figure S11. (a) Polarization curves and (b) overpotentials of various V-CoP samples at 10 mA cm^{-2} for HER. (c) Polarization curves and (d) overpotentials of various Fe-CoP samples at 10 mA cm^{-2} for HER.

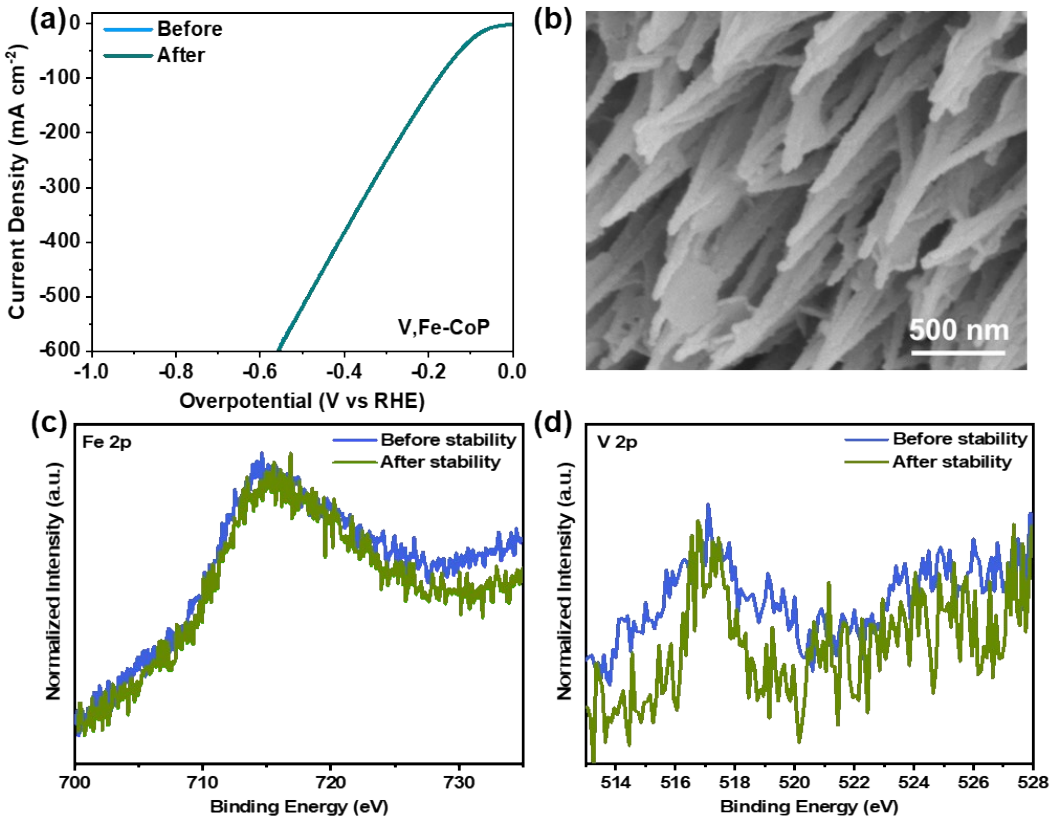

Figure S12. (a) LSV curves of V,Fe-$Co_{5.47}N$ before and after the HER stability test. (b) SEM image of V,Fe-$Co_{5.47}N$ after stability test. (c) Fe 2p and (d) V 2p of V, Fe-$Co_{5.47}N$ after HER stability test.

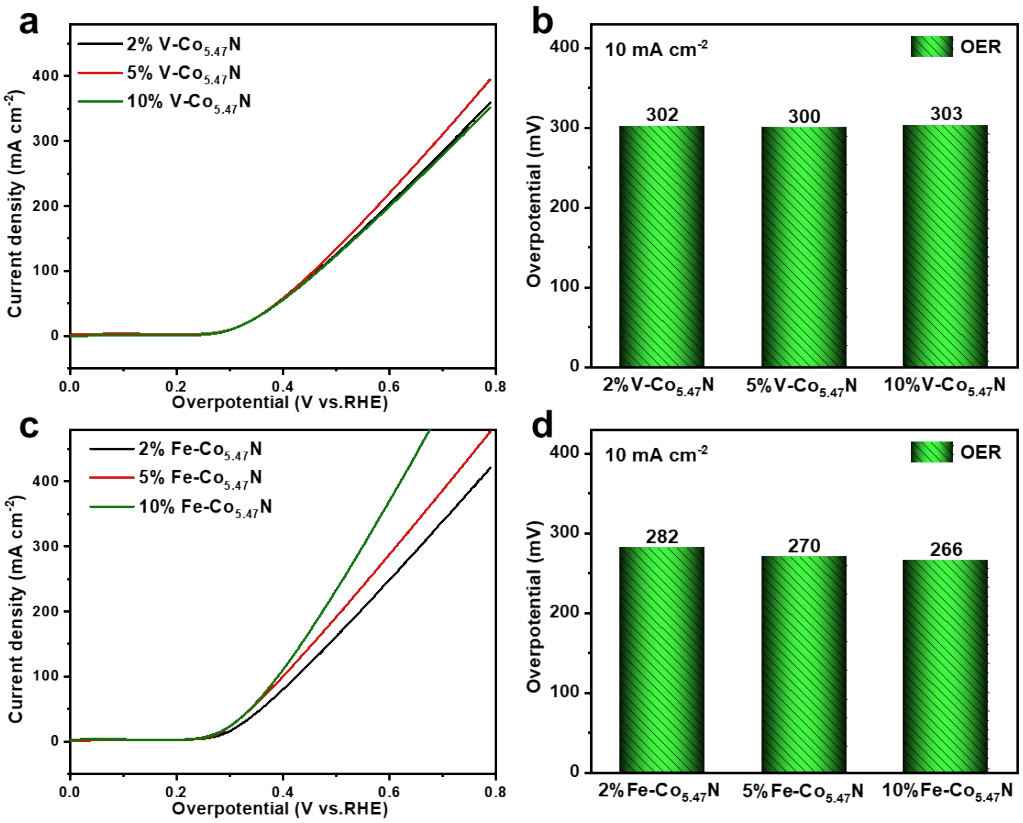

Figure S13. (a) Polarization curves and (b) overpotentials of various V-$Co_{5.47}N$ samples at 10 mA cm^{-2} for OER. (c) Polarization curves and (d) overpotentials of various Fe-$Co_{5.47}N$ samples at 10 mA cm^{-2} for OER.

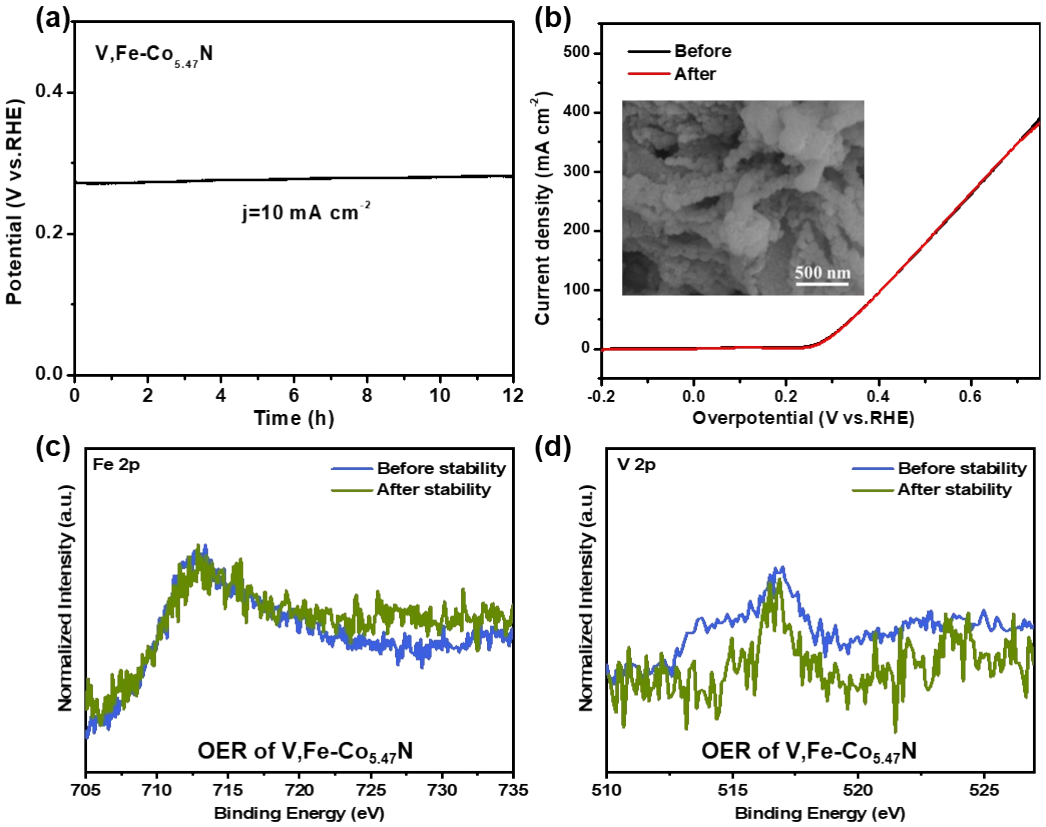

Figure S14. (a) Stability test for HER of V,Fe-$Co_{5.47}$N electrocatalyst at current density of 10 mA cm^{-2}. (b) LSV curves of V,Fe-$Co_{5.47}$N before and after the HER stability test. Inset is the SEM image of V,Fe-$Co_{5.47}$N after stability test. (c) Fe 2p and (d) V 2p of V, Fe-$Co_{5.47}$N after HER stability test.

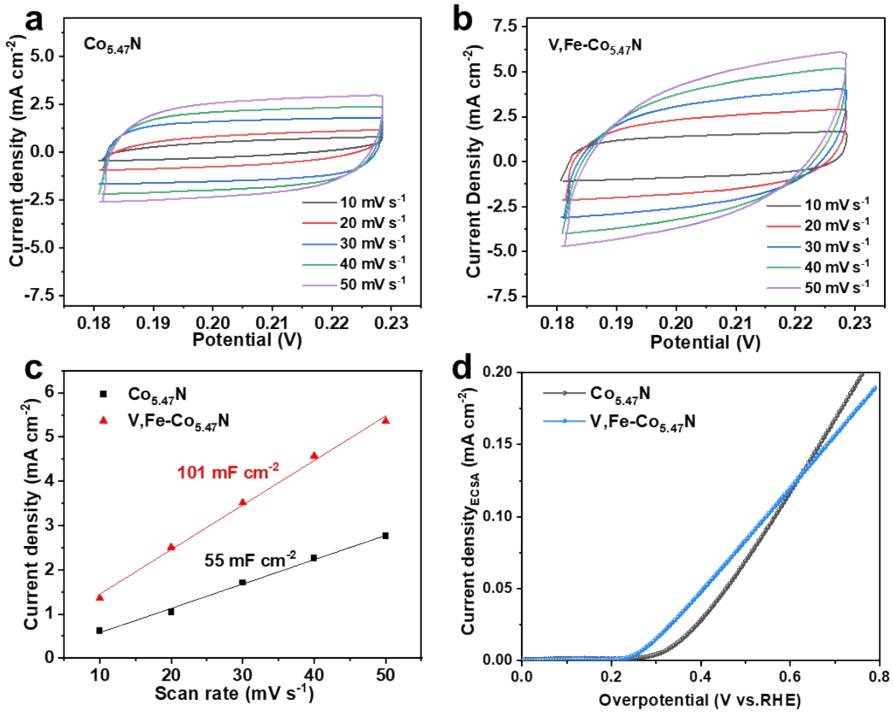

Figure S15. CV curves (a) $Co_{5.47}N$ and (b) V,Fe-$Co_{5.47}N$ in the double layer capacitive region at the scan rates of 10 mV s^{-1} to 50 mV s^{-1} for OER. (c) Current density as a function of scanning rate for HER of $Co_{5.47}N$ and V,Fe-$Co_{5.47}N$. (d) OER Normalized ECSA.

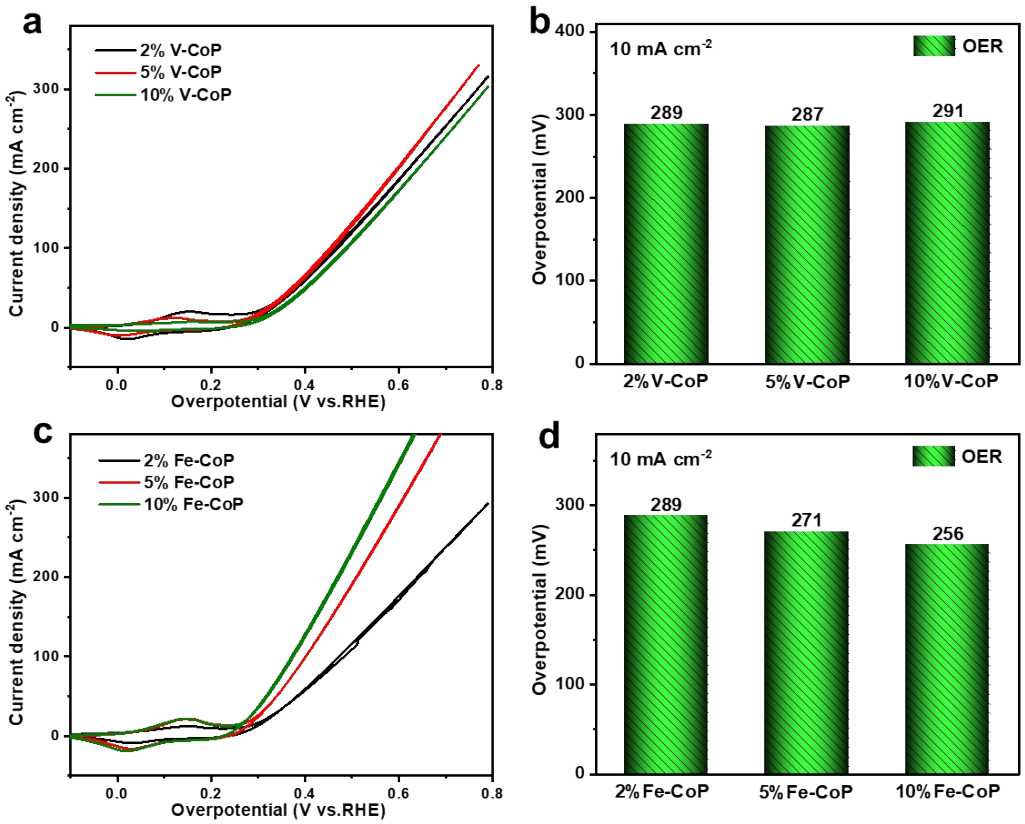

Figure S16. (a) Polarization curves and (b) overpotentials of various V-CoP samples at 10 mA cm^{-2} for OER. (c) Polarization curves and (d) overpotentials of various Fe-CoP samples at 10 mA cm^{-2} for OER.

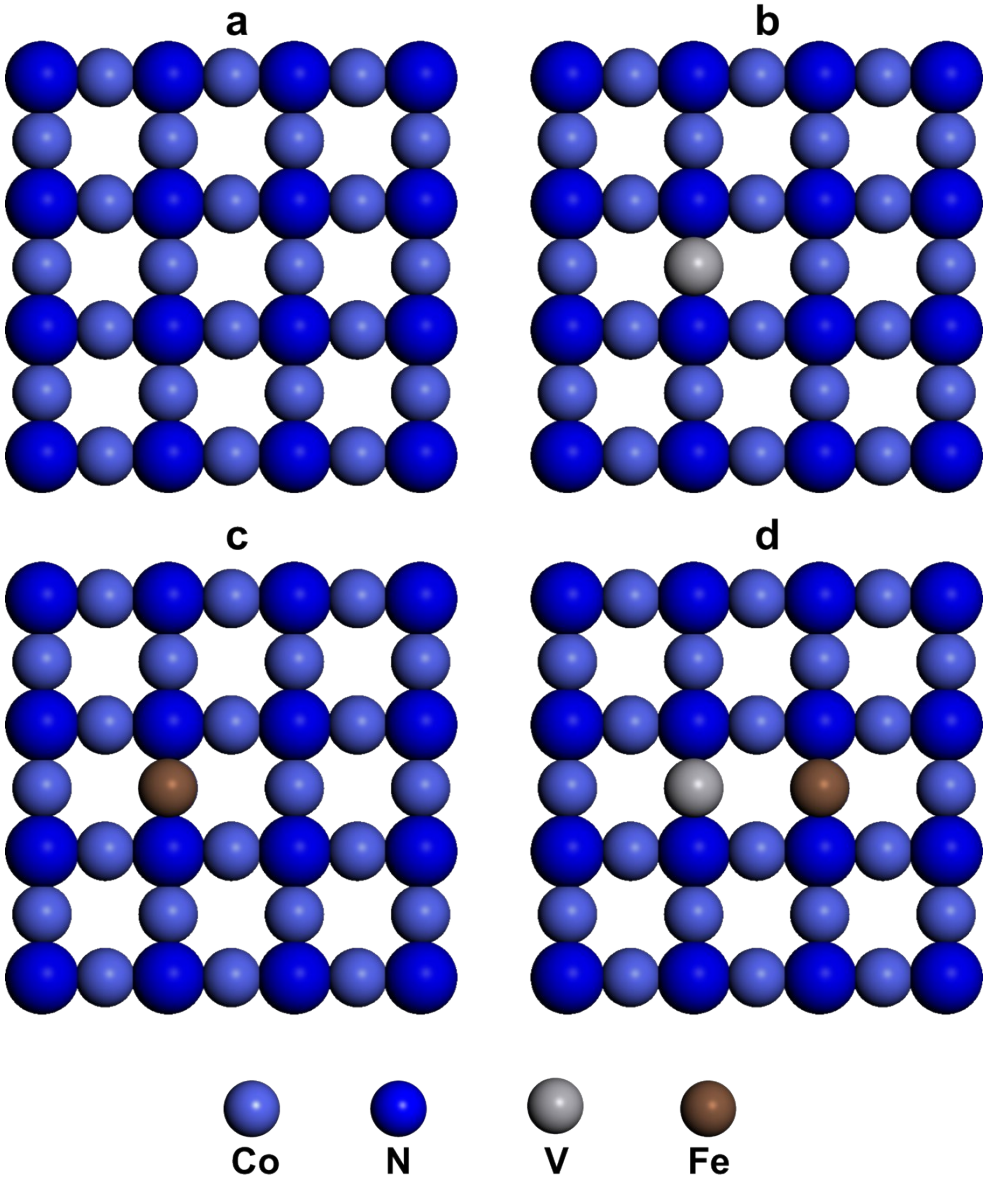

Figure S17. Optimized structural models of the (200) plane of $Co_{5.47}N$, V-$Co_{5.47}N$, Fe-$Co_{5.47}N$, and V,Fe-$Co_{5.47}N$.

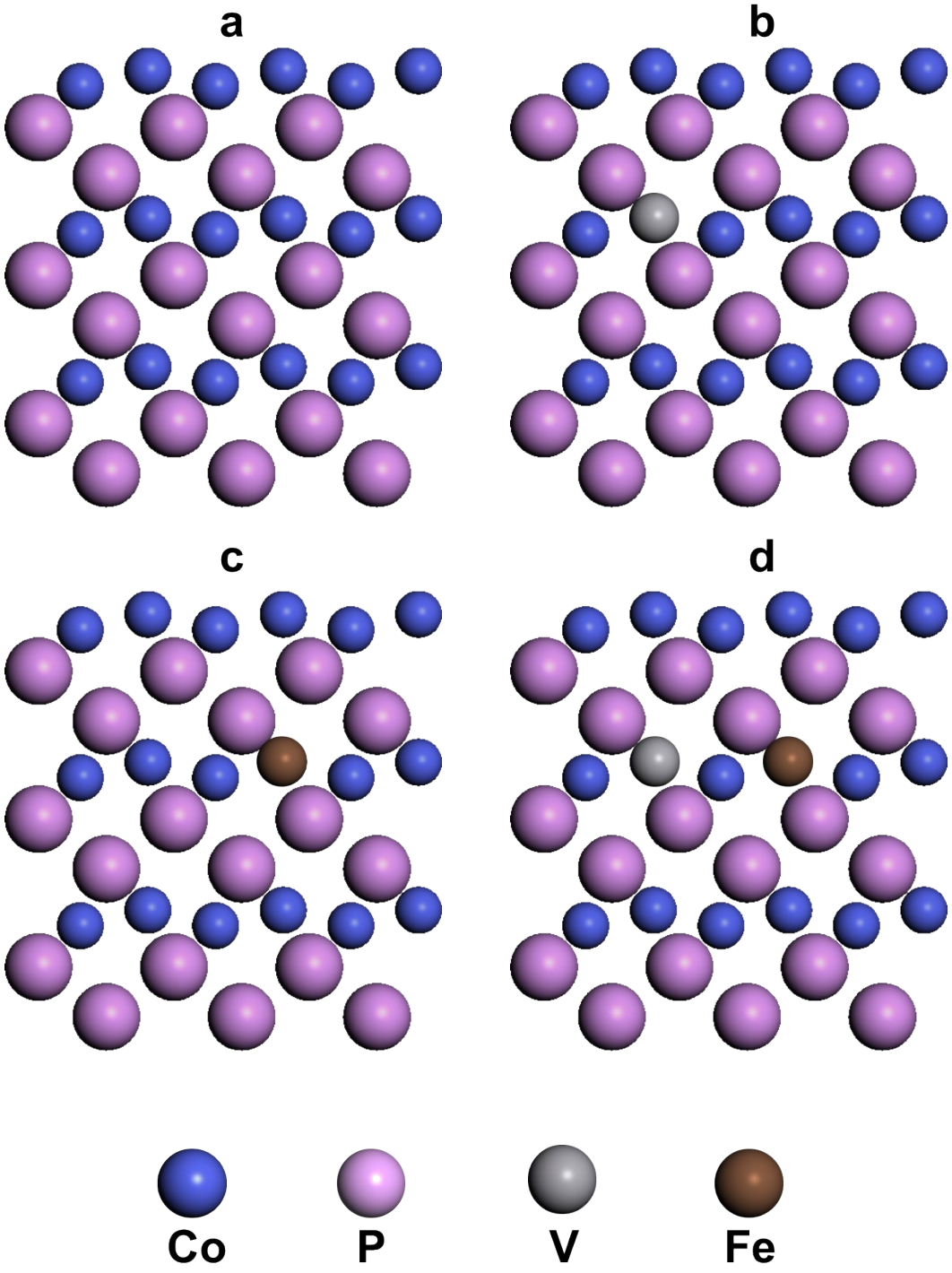

Figure S18. Optimized structural models of CoP, V-CoP, Fe-CoP, and V,Fe-CoP.

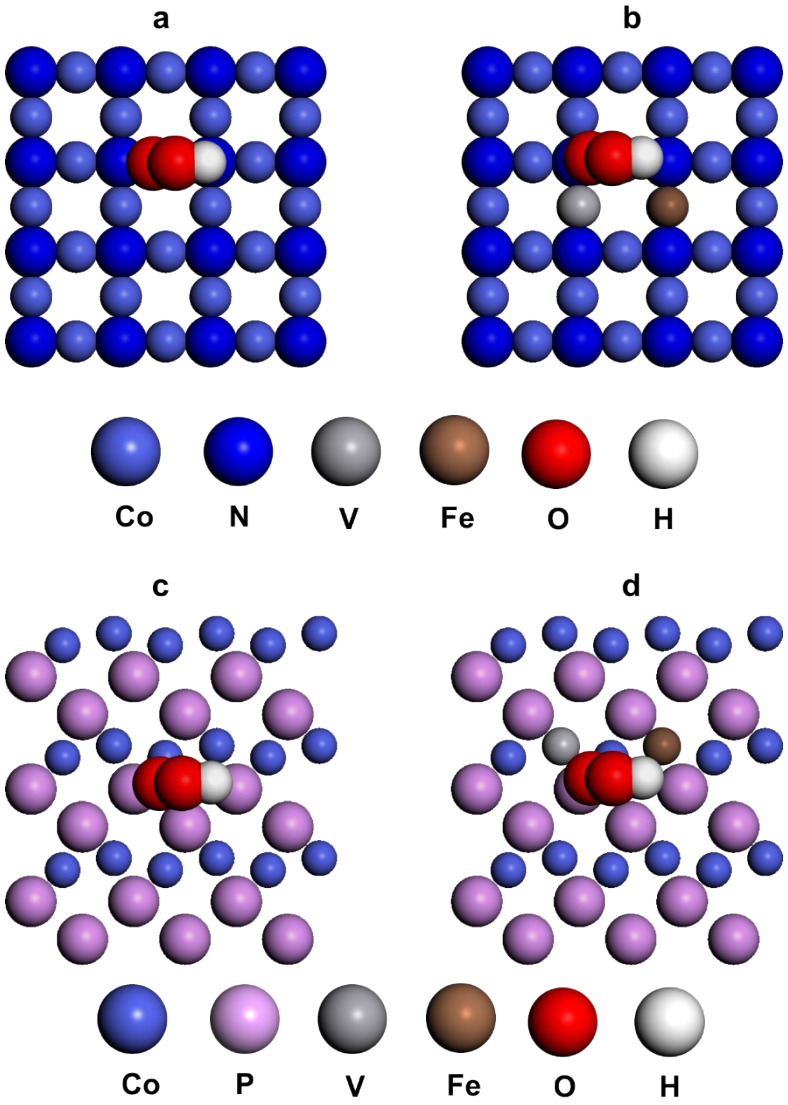

Figure S19. The structural model of *OOH adsorption on (a) $Co_{5.47}N$, (b) V,Fe-$Co_{5.47}N$, (c) CoP, and (d) V,Fe-CoP (down).

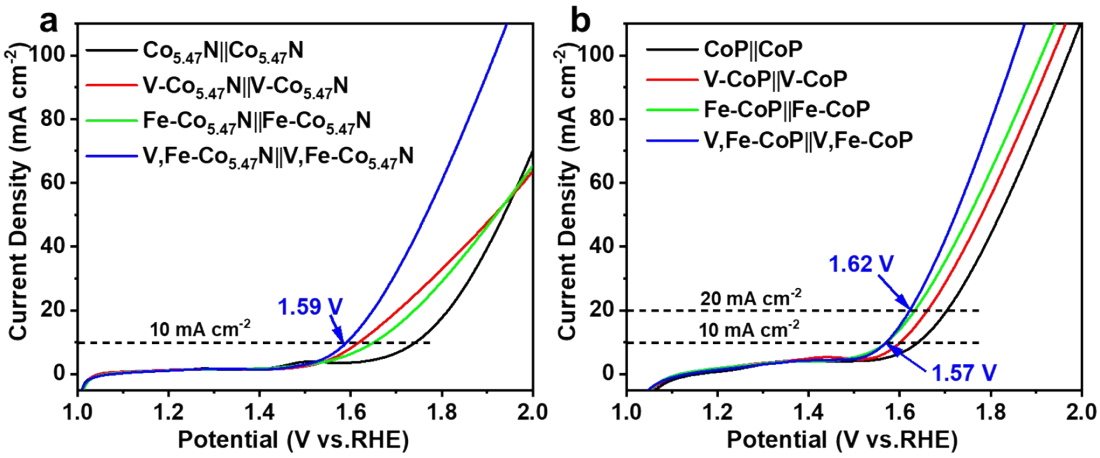

Figure S20. LSV curves of bifunctional (a) $Co_{5.47}N$-based and (b) CoP-based OWS devices.